

Properties of polyacrylic acid-coated silver nanoparticle ink for inkjet printing conductive tracks on paper with high conductivity

Qijin Huang ^a, Wenfeng Shen ^{a,*}, Qingsong Xu ^a, Ruiqin Tan ^b, Weijie Song ^{a,*}

^a Ningbo Institute of Material Technology and Engineering, Chinese Academy of Sciences, Ningbo, Zhejiang 315201, China

^b Faculty of Information Science and Engineering, Ningbo University, Ningbo, Zhejiang 315211, China

HIGHLIGHTS

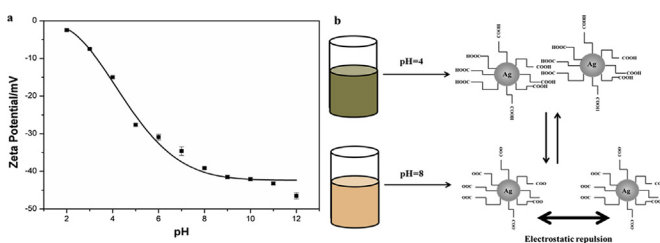
- An ink from silver nanoparticles coated with polyacrylic acid was prepared.
- The ink was used for inkjet-printed tracks at varying printing parameters.
- The conductivity of printed tracks sintered at 150 °C increased to 2.1×10^7 S/m.
- Mechanism for dispersion and aggregation of the nanoparticles in ink is discussed.

ARTICLE INFO

Keywords:

- A. Electronic materials
- B. Sintering
- C. Electron microscopy
- D. Electrical properties

GRAPHICAL ABSTRACT



ABSTRACT

Silver nanoparticles with a mean diameter of approximately 30 nm were synthesized by reduction of silver nitrate with triethanolamine in the presence of polyacrylic acid. Silver nanoparticle-based ink was prepared by dispersing silver nanoparticles into a mixture of water and ethylene glycol. The mechanism for the dispersion and aggregation of silver nanoparticles in ink is discussed. The strong electrostatic repulsions of the carboxylate anions of the adsorbed polyacrylic acid molecules disturbed the aggregation of metal particles in solutions with a high pH value (pH > 5). An inkjet printer was used to deposit this silver nanoparticle-based ink to form silver patterns on photo paper. The actual printing qualities of the silver tracks were then analyzed by variation of printing passes, sintering temperature and time. The results showed that sintering temperature and time are associated strongly with the conductivity of the inkjet-printed conductive patterns. The conductivity of printed patterns sintered at 150 °C increased to 2.1×10^7 S m⁻¹, which was approximately one third that of bulk silver. In addition, silver tracks on paper substrate also showed better electrical performance after folding. This study demonstrated that the resulting ink-jet printed patterns can be used as conductive tracks in flexible electronic devices.

1. Introduction

In the last few years, there has been growing interest in inkjet printing for use in various applications [1–4]. The advantages of inkjet printing include the ease with which it can be used to form

high-speed pattern, its low cost, and its applicability to various substrates [5–8]. Inkjet printing is particularly attractive technology to manufacture devices on flexible substrates [9,10]. In all flexible substrates, paper is by far the cheapest and most widely used in daily life, and paper has gained attention because of it is recyclable, lightweight, and biodegradable [11,12], leaving a negligible environmental footprint [13]. Inkjet printing is particularly attractive for realizing direct metallization on paper substrate in fabrication of electronic circuits or devices because most of

* Corresponding authors.

E-mail addresses: wfshen@nimte.ac.cn (W. Shen), weijiesong@nimte.ac.cn (W. Song).

electronic devices require contacts and conductive structures, and metals are the primary choices due to their high conductivity [14]. Applications include radio frequency identification tags (RFIDs) [15,16], sensors [17], electronic circuits [18], RF energy harvesting and wireless power transmission devices [19].

To successfully produce metal tracks and patterns on paper substrates by inkjet printing, stable metal inks with high quality were needed to be produced. Metals inks based on metal nanoparticles and organometallic precursors are two choices [20,21]. Metal nanoparticle-based inks are advantageous for use on paper due to the limited penetration of metal particles into this porous substrate. The metals that have been developed for use in nanoparticle-based inks include gold (Au) [22–24], silver (Ag) [25], and copper (Cu) [26–28]. Because bulk silver has the lowest resistivity ($1.6 \mu\Omega \text{ cm}$), and because copper nanoparticles oxidize spontaneously in air [29] and gold is expensive, silver has been most widely used and reported.

Different capping agents are used to tailor silver nanoparticle properties. Short chain carboxylic acids (C_6 – C_{10}) [30], poly(vinyl pyrrolidone) (PVP) [31,32], and polyacrylic acid (PAA) [33] have been used as surface-capping molecules to control the particle size. It is important to study the mechanism for the dispersion and aggregation of silver nanoparticles to improve the stability of silver ink. Additionally, it is necessary to sinter printed patterns to remove the organic residues and produce highly conductive structures. The sintering temperature may affect the properties of flexible substrates, especially paper. However, silver nanoparticles can exhibit good conductivity when sintered at approximately 200°C – 350°C [34,35], which is incompatible with many plastic and paper substrates used in flexible electronics. In order to shorten sintering time and lower sintering temperature, several sintering methods, which can be performed even at room temperature, were recently developed based on coalescence of metal NPs triggered by chemical agents [36], such as NaCl [37] and HCl vapor [38].

In this study, we report the preparation of inks containing well-dispersed polyelectrolyte-capped silver nanoparticles. Additionally, we studied the mechanism for the dispersion and aggregation of the silver nanoparticle-based ink. We also investigated the influence of printing passes, sintering temperature and time on the electrical resistivity and morphology of inkjet-printed patterns. The application of stable silver nanoparticle-based ink in conductive patterns was also presented.

2. Experimental section

2.1. Materials

All of the chemical reagents used in these experiments were purchased from commercial sources with analytical purity and used without further purification. Silver nitrate (AgNO_3), triethanolamine (TEA), ethanol, ethylene glycol (EG), and nitric acid (HNO_3) were purchased from Sinopharm Chemical Reagent Co., Ltd. Polyacrylic acid (PAA, MW ~3000) and 2-amino-2-methyl-1-propanol (AMP) were purchased from Aladdin Industrial Inc. Deionized water was used in all of these experiments. Kodak premium photo paper (“photo paper” for short) was used as the paper substrate. This photo paper consists of 9 layers and the root-mean-square (RMS) roughness of the photo paper is 18 nm [39] (More detailed description of the photo paper, see Supporting information).

2.2. Preparation of silver nanoparticles and inks

In a typical synthesis, 10 g AgNO_3 was dissolved in 10 g deionized water in a beaker with stirring to form a colorless and

transparent solution. Then, a mixture (pH ~ 9) of 0.25 g PAA, 30 g TEA and 20 g deionized water was added dropwise to AgNO_3 solution with continuous magnetic stirring. The reaction mixture was stirred for 24 h. Next, the products were precipitated by adding ethanol. To remove the unreacted organic and metal salts, the mixture was filtered and washed with copious amounts of ethanol. Finally, the silver nanoparticles were dried at 60°C . The solid form of silver nanoparticles can be stored and transported conveniently.

Silver nanoparticle-based ink with a solids loading of 20 wt% was prepared by adding a mixture of ethylene glycol and water (3:7 by weight) to the silver nanoparticles. The viscosity and surface tension of this as-prepared silver nanoparticle-based ink were 5.46 mPa s and 41 mN m^{-1} , respectively.

2.3. Fabrication and treatment of silver patterns

Silver patterns were deposited on photo paper by inkjet printing technology, which was similar to the technique used in our previous work [40]. Inkjet printing was performed with a common color printer (Epson Stylus Photo R230), whose print head has 6 rows of orifices, with each row feature 90 orifices measuring approximately $28 \mu\text{m}$ in diameter. Although the printer has six ink containers, we use only one the container intended for black ink for our silver ink in this study. The silver nanoparticle-based ink was ultrasonically for 10 min, filtered through $0.22 \mu\text{m}$ membrane and loaded into the cartridges. The ink was printed onto paper, and the bead was air-dried for 5 min between printings. The inkjet-printed silver patterns were sintered at various temperatures between 25°C and 150°C for 10 min in air.

2.4. Characterization

Structural characterization of silver nanoparticles was carried out using X-ray diffraction (XRD) with a Bruker AXS D8 Advance diffractometer with $\text{Cu K}\alpha$ radiation ($\lambda = 0.1542 \text{ nm}$). The morphology and size of as-synthesized silver nanoparticles were characterized by transmission electron microscopy (TEM, Tecnai, F20, 200 KV). The texture of silver tracks was measured with Leica DM 2500 optical microscopy (OM). Particle sizes were evaluated by dynamic light scattering (DLS), and zeta-potential analyses were performed using a Zetasizer nano-SZ (Malvern Instruments). The surface morphology and thickness of the silver lines were observed with a Hitachi S-4800 field emission scanning electron microscope (FESEM) using an operating voltage of 8 kV. The electrical resistivity of the silver patterns was detected by a 4-point probe system (Lucas-Signatone Pro4-4000) and calculated using the geometric dimensions of the patterns.

3. Results and discussion

3.1. Properties of silver nanoparticles

Fig. 1 presents the scheme for the synthesis of silver nanoparticles from silver nitrate. TEA and PAA were used as reducing agent and capping agent, respectively. After adding TEA and PAA to silver nitrate solution, the mixture undergoes a gradual change from colorless to dark black, which coincides with the nucleation and growth of silver nanoparticles. When TEA and PAA were added gradually to AgNO_3 solution, the reduction of Ag^+ proceeded slowly, and then the concentration of Ag^0 approached the critical concentration for nucleation. When nucleation occurs, some Ag^0 species convert to nuclei, some Ag^+ are reduced continuously to Ag^0 , and the nucleation step continues for a relatively long period of time. As the silver nanoparticles grow, the mixture gradually becomes dark and turbid because large particles reflect and scatter

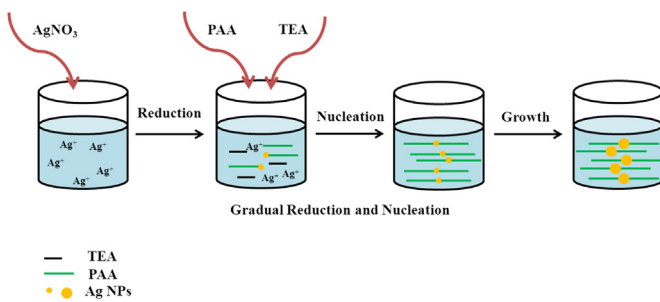


Fig. 1. Schematic illustration of the preparation of silver nanoparticles. Poly(acrylic acid) was used to stabilize the silver nanoparticles.

more light than small ones. After 24 h, the color of the mixture stops changing, which indicates the termination of nanoparticle growth. After the reaction is complete, ethanol is added to precipitate the products. Ethanol, a poor solvent for PAA-coated nanoparticles, can induce rapid particle coagulation. After filtering and washing, silver nanoparticles can be dried for ease of use and storage.

The X-ray diffraction pattern of the prepared silver nanoparticles, presented in Fig. 2a, shows the peaks that are characteristic of metallic silver. According to the Silver Joint Committee on Powder Diffraction Standards Database (File NO. 04-0783), the

reflection peaks are indexed as fcc (111), (200), (220), and (311) planes, indicating that silver is well crystallized. This result shows that the synthesized silver nanoparticles consist of a pure Ag phase without secondary phases such as byproducts or oxide phases. The morphology and the size distribution of the silver nanoparticles were studied by TEM. Fig. 2b shows a TEM image of a near-complete monolayer of silver nanoparticles, where most of the particles have a spherical shape and a narrow size distribution with an average size of 30 nm. More details are revealed in the HRTEM image (Fig. 2c). The bright amorphous layer, approximately 1 nm thick, along the edge of the silver nanoparticle is most likely PAA. These organic surface layers act as insulating barriers and stabilize the nanosized particles.

3.2. Mechanism for dispersion and aggregation of silver nanoparticle ink

For electrolyte-coated Ag nanoparticles, the pH value significantly impacts the stability of silver nanoparticle-based ink. To investigate the relationship between pH and the dispersion–aggregation of PAA-coated nanoparticles, silver nanoparticles were thoroughly dispersed in DI-water without incorporating any additional dispersants. The pH value of the aqueous silver ink was adjusted by adding HNO_3 or AMP.

To estimate the electrical charge at the surface of Ag nanoparticles, the effect of pH on the zeta potential (ζ) of the silver ink

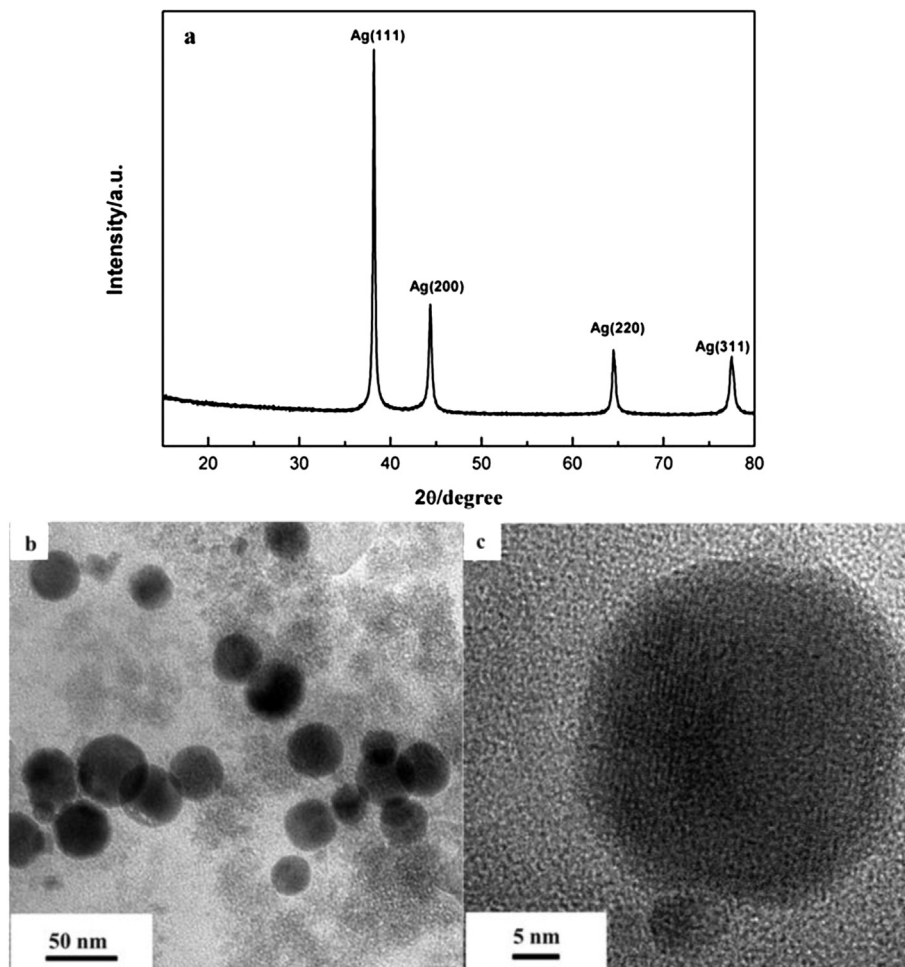


Fig. 2. (a) XRD pattern of Ag nanoparticles after drying at 60 °C. (b) TEM and (c) HRTEM images of Ag nanoparticles. The measured average particle size is 30 nm.

has been investigated, and the results are shown in Fig. 3a. Fig. 3a shows the pH value significantly impacts the stability of silver nanoparticle-based ink. With the increase of pH value, zeta potential $|\zeta|$ also increase, which is the reason of electrostatic stabilization mechanism [41]. The surfaces of silver nanoparticles in solution were negatively charged when the pH was larger than 5, but the electric charge decreased when the pH was less than 5 and approached zero at pH = 2. From these observations of the zeta potential, a pH-dependent mechanism of dispersion and aggregation of silver particles can be proposed as showed shown in Fig. 3b. The carboxylic group of polyacrylic acid adsorbs on silver particles by forming Ag–OCO⁻ bonds as a protective agent. At pH values above 5, the proton of the terminal carboxylic group electrolytically dissociates to form a carboxylate anion, and a negative electrical potential forms on the surface of silver nanoparticles. The silver nanoparticles with a negative surface charge are highly dispersed without aggregation because of the electrostatic repulsion between the silver nanoparticles. In this case, the layer of polymeric dispersant molecules absorbed on the particles surfaces acted as an effective layer for steric stabilization to prevent them from

agglomerating. At a pH below 5, the silver surface is electrostatically neutral, the proton of the weakly acidic carboxylic acid group of adsorbed polyacrylic acid cannot be ionized, the driving force for dispersion is lost, and the silver nanoparticles undergo aggregation. The DLS results show that the silver particles size at pH = 5 is approximately 45 nm, and the size increases to 1190 nm at pH = 4 (Fig. S1, Supporting information). Thus, AMP was added to the final silver nanoparticle-based ink to maintain the pH near 9.

3.3. Preparation of silver patterns on photo paper with different parameters

An inkjet printer was used to form silver tracks with different printing passes (N) and setting widths (λ). Fig. 4 shows optical microscope images of the actual widths of printed lines compared with the widths set by Microsoft Word, where the number of printing passes was ten. Although the width was set at 0 pt in Microsoft Word, we clearly obtained lines of 282 μm with many breaks. When the set widths ranged from 0.25 pt (88 μm) to 1.5 pt (528 μm), the actual widths increased from 350 μm to 856 μm . The actual widths observed under the optical microscope were greater than the settings.

The actual widths of printed lines with different printing passes, and the set width of 1 pt (352 μm) are shown in Fig. S2 (Supporting information). When printing only once, the actual width was 410 μm , which was a little wider than the setting value. However, when printing 10 times, the actual width was 635 μm , which was 1.8 times the setting value. Thus, in practical applications, we can produce the required width by changing the setting widths (λ) or the number of printing passes (N). This discrepancy between the setting value and the actual width can vary with the substrate because it depends on the composition and surface properties of the substrate.

We speculate about the conductive mechanism of the printed patterns. When the silver inks were ejected from the orifice of the inkjet printer, a single ink droplet produced an irregular spherical dot pattern on the paper substrate. As shown in Fig. 5, the single silver dot pattern was approximately 80 μm in diameter. The silver track cannot be conductive if the track consists of only single dots. When printing repeatedly, the distance between dots decreased. The droplets between dots had more overlap and formed a continuous line. The silver track with relatively smooth edge definition became conductive.

Fig. 6 shows SEM images of track thickness with different printing passes: (a) $N = 10$ and (b) $N = 15$. The thickness of the silver tracks increased with printing passes because more inks was applied during printing. When printing 10 times, the approximate thickness was 500 nm (Fig. 6a), and the line was more dense. The thickness increased to 750 nm when the printing passes was 15. The line is somewhat wrinkled because of shrinkage after thermal treatment.

3.4. Electrical and mechanical properties of silver patterns printed on photo paper

The resistivity generally decreased with increasing the heating temperature or time, showing a sintering effect for nanosized silver colloids in the ink [42,43]. Fig. 7 shows the SEM pictures of surface morphology after different temperature treatments for 10 min each. The sintering effect with temperature is visible. At 25 °C, each silver particle appeared to be unchanged and was observed clearly. Yet, after heating at 50 °C for 10 min, the sintering effect became obvious, and the size of particles increased significantly. These critical changes in morphology with the formation of continuous interconnections between particles are seen at temperature as low

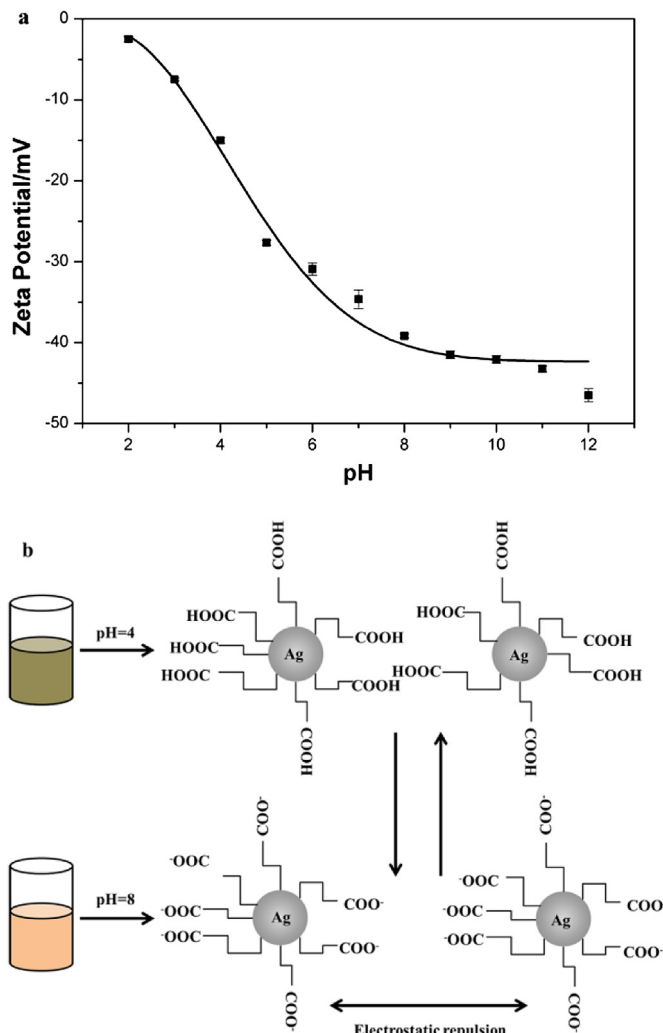


Fig. 3. (a) Zeta-potential of Ag nanoparticles as a function of pH of an aqueous medium. The solid line represents the non-linear regression and the points denote experimental results. (b) The mechanism for the dispersion–aggregation of the Ag nanoparticles-based ink. This test was carried out to determine the proper pH value of silver nanoparticle-based ink.

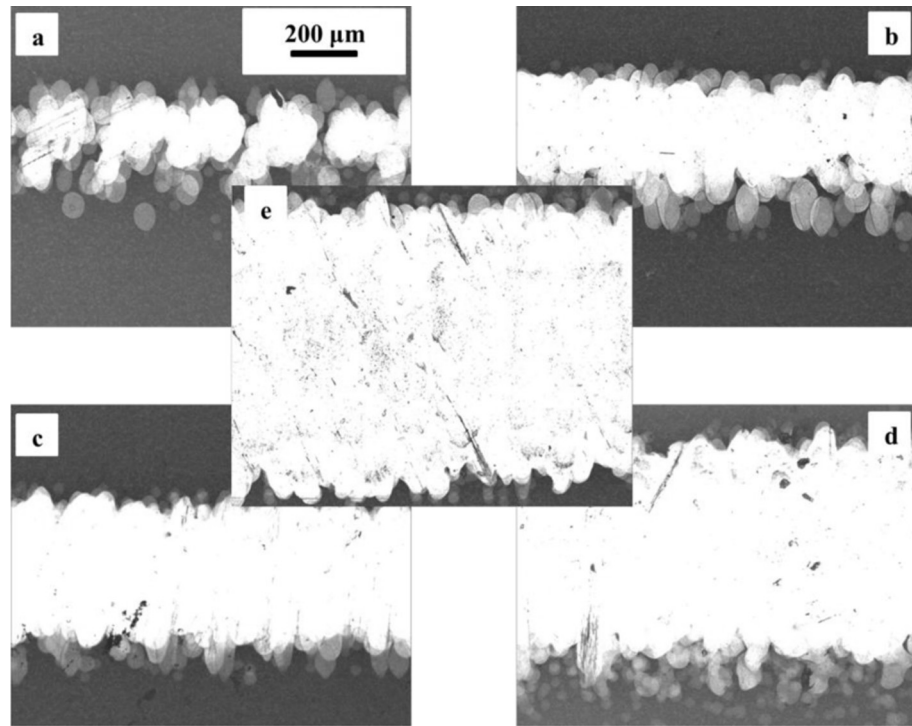


Fig. 4. Optical microscope images of actual silver tracks width in comparison with defined line widths for printed ten times: (a) 0 pt, (b) 0.25 pt, (c) 0.5 pt, (d) 1 pt, and (e) 1.5 pt. The orifice diameter of the nozzle used here was 28 μm .

as 80 °C. Most boundaries between particles disappeared due to sintering and the formation of continuous interconnections, and thus the electrical resistivity decreased to low values. When the sintering temperature reaches 150 °C, most of the nanoparticles have fused together to form a network throughout the entire silver

film. Some voids and cracks formed on the surface of the track after sintering at 150 °C. This behavior is attributed primarily to the residual thermal stresses that build up in the lines upon cooling due to the different thermal expansion coefficients for silver lines and the paper coating.

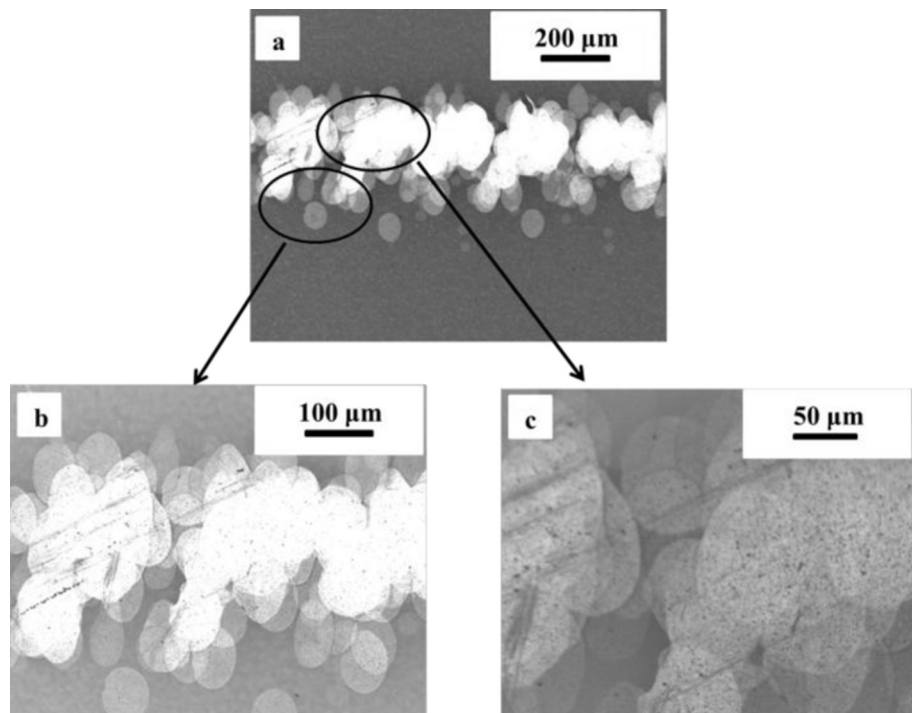


Fig. 5. Optical microscope images of printed Ag tracks with different magnifications. The magnified images for parts of Ag tracks are shown in (b) and (c).

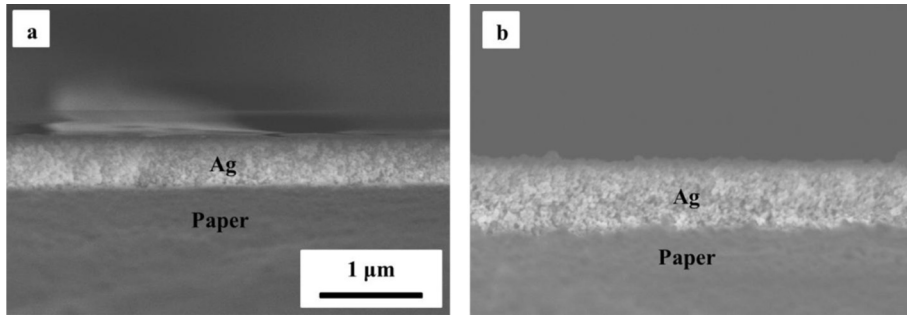


Fig. 6. SEM images of track thickness for different printing passes: (a) $N = 10$ and (b) $N = 15$. The track thickness increase with printing passes.

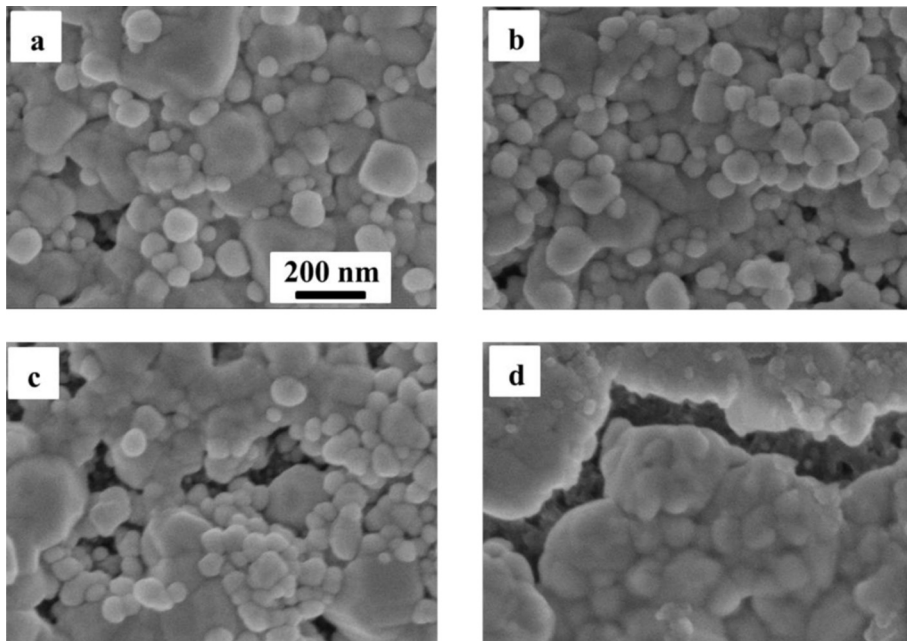


Fig. 7. SEM images of the surface morphology after different temperature treatments: (a) 25 °C, (b) 50 °C, (c) 80 °C, and (d) 150 °C. The sintering effect with temperature can be seen from the surface morphology change.

In Fig. 8, the measured resistivity of the silver films on paper is shown as a function of the sintering temperature. After sintering at room temperature (25 °C), the resistivity of the silver films was 12.6 $\mu\Omega \text{ cm}$. This self-sintering phenomenon of the Ag nanoparticles was due to the polymer coating on the paper substrate. Upon sintering at 150 °C, the resistivity of the printed silver patterns decreased to 4.7 $\mu\Omega \text{ cm}$, which is close to triple that of bulk silver. To avoid degradation of the paper substrate, lower temperature or shorter sintering time should be used, resulting in a relatively larger resistivity, such as the resistivity of the silver patterns sintering at 60 °C for 10 min, which was 9 $\mu\Omega \text{ cm}$. Moreover, the silver films attached to the paper substrate fairly well. A simple tape test was performed to examine the adhesion of silver films. The silver films stayed on the paper surfaces completely after removal of the attached tape (Scotch tape, 3 M), indicating good adhesion between the printed silver films and paper substrate. SEM images of Ag films before and after tape test were shown in Fig. S3 (Supporting information).

To illustrate the mechanical flexibility of inkjet-printed silver tracks on paper, a folding test was performed by folding the test specimens to $\pm 180^\circ$. The test specimen was folded to -180° (or $+180^\circ$) and released back to 0° . The electrical resistance of silver

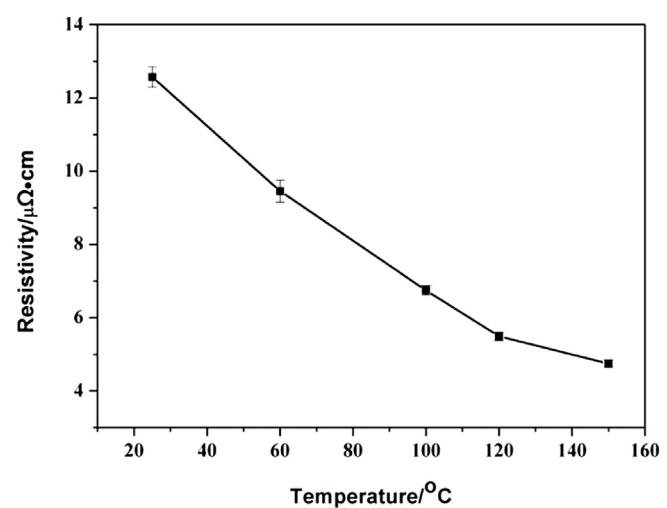


Fig. 8. Resistivity of Ag patterns printed on paper substrate as a function of the sintering temperature. The points denote experimental results and the solid line represents the connection between the points.

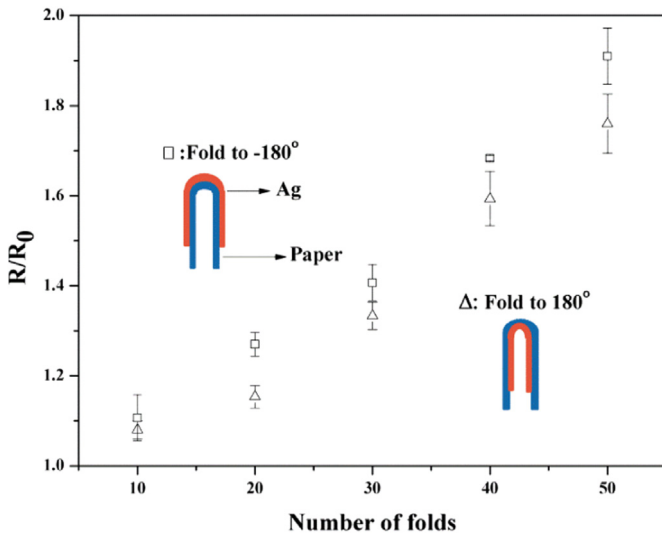


Fig. 9. Variations in the electrical resistance of Ag tracks on paper as a function of $\pm 180^\circ$ folding cycles. The measured electrical resistance at the designated fold cycle and the initial resistance in the as-printed state are R and R_0 , respectively. The test specimen was folded to -180° (or $+180^\circ$) and released back to 0° .

tracks was measured every 10 cycles. As shown in Fig. 9, the electrical resistance of the printed Ag tracks increased gradually with repeated folding of the test specimens. These resistances vary less than twice the resistance of the original printed silver tracks, even after folding 50 cycles, which indicates that the well-encapsulated printed silver tracks on paper can satisfy the requirements of flexible circuits. For example, these as-printed narrow silver tracks can be used in flexible electronic applications such as radio frequency identification (RFID) tags or electrodes for thin-film transistor (TFT) circuits. To demonstrate the applicability of the silver nanoparticles-based ink for inkjet printing electronics, LED connected circuits were printed on paper and the fabricated LED devices showed good flexibility, as shown in Fig. S4 (Supporting information).

4. Conclusions

In summary, by using triethanolamine as the reducing agent and polyacrylic acid as the protective agent, silver nanoparticles can be synthesized from an aqueous solution of AgNO_3 . The mechanism for the dispersion and aggregation of the silver nanoparticle-based ink is discussed. The polyacrylic acid adsorbed on the surfaces of nano-sized silver particles prevented the aggregation of silver nanoparticles and controlled their particle size. Using this silver nanoparticle-based ink, silver patterns could be deposited on photo paper by inkjet printing. The resistivity of these printed patterns sintered at 150°C was close to triple the resistivity of the bulk silver. Additionally, these silver tracks on paper showed better electrical performance after folding, and they can serve as conducting tracks in flexible electronic devices.

Acknowledgments

This work has been supported by the National Natural Science Foundation of China (Grant no. 21205127, 61275114), the Zhejiang Provincial Natural Science Foundation of China (Grant no. LY12E02009) and the Ningbo Innovative Research Team Program (2009B21005, 2011B82005).

Appendix A. Supplementary data

Supplementary data related to this article can be found at <http://dx.doi.org/10.1016/j.matchemphys.2014.05.030>.

References and notes

- [1] K.-W. Park, S.-B. Kang, J.-A. Jeong, S.-W. Choi, J. Kim, I.-K. You, Y.S. Yang, H.-K. Kim, *J. Phys. D Appl. Phys.* 46 (2013) 145301.
- [2] J.L. Zhuang, D. Ar, X.J. Yu, J.X. Liu, A. Terfort, *Adv. Mater.* 25 (2013) 4631–4635.
- [3] M. Fang, A. Aristov, K.V. Rao, A.V. Kabashin, L. Belova, *RSC Adv.* 3 (2013) 19501–19507.
- [4] A. Kosmala, Q. Zhang, R. Wright, P. Kirby, *Mater. Chem. Phys.* 132 (2012) 788–795.
- [5] H.H. Lee, K.S. Chou, K.C. Huang, *Nanotechnology* 16 (2005) 2436–2441.
- [6] J.-T. Wu, S.-L.-C. Hsu, M.-H. Tsai, W.-S. Hwang, *J. Phys. Chem. C* 115 (2011) 10940–10945.
- [7] D. Soltman, V. Subramanian, *Langmuir* 24 (2008) 2224–2231.
- [8] P.J. Smith, A. Morrin, *J. Mater. Chem.* 22 (2012) 10965–10970.
- [9] D. Mager, A. Peter, L. Del Tin, E. Fischer, P.J. Smith, J. Hennig, J.G. Korvink, *IEEE Trans. Med. Imaging* 29 (2010) 482–487.
- [10] P.Q. Nguyen, L.P. Yeo, B.K. Lok, Y.C. Lam, *ACS Appl. Mater. Interfaces* 6 (2014) 4011–4016.
- [11] A. Russo, B.Y. Ahn, J.J. Adams, E.B. Duoss, J.T. Bernhard, J.A. Lewis, *Adv. Mater.* 23 (2011) 3426–3430.
- [12] D. Töbjörk, R. Österbacka, *Adv. Mater.* 23 (2011) 1935–1961.
- [13] A. Kamshny, S. Magdassi, *Small* (2014), <http://dx.doi.org/10.1002/smll.201303000>.
- [14] S.F. Jahn, T. Blaudeck, R.R. Baumann, A. Jakob, P. Ecorchard, T. Rüffer, H. Lang, P. Schmidt, *Chem. Mater.* 22 (2010) 3067–3071.
- [15] V. Lakafosis, A. Rida, R. Vyas, L. Yang, S. Nikolaou, M.M. Tentzeris, in: *Proc. IEEE* 98, 2010, pp. 1601–1609.
- [16] A. Rida, L. Yang, R. Vyas, M.M. Tentzeris, *IEEE Antennas Propag. Mag.* 51 (2009) 13–23.
- [17] S. Kim, B. Cook, T. Le, J. Cooper, H. Lee, V. Lakafosis, R. Vyas, R. Moro, M. Bozzi, A. Georgiadis, *IET Microw. Antennas Propag.* 7 (2013) 858–868.
- [18] A.C. Siegel, S.T. Phillips, M.D. Dickey, N. Lu, Z. Suo, G.M. Whitesides, *Adv. Funct. Mater.* 20 (2010) 28–35.
- [19] S. Kim, R. Vyas, A. Georgiadis, A. Collado, M.M. Tentzeris, in: *Microwave Conference (EuMC), 2013 European, IEEE*, 2013, pp. 983–986.
- [20] D. Deng, Y. Jin, Y. Cheng, T. Qi, F. Xiao, *ACS Appl. Mater. Interfaces* 5 (2013) 3839–3846.
- [21] P.J. Smith, D.Y. Shin, J.E. Stringer, B. Derby, N. Reis, *J. Mater. Sci.* 41 (2006) 4153–4158.
- [22] N. Zhao, M. Chiesa, H. Sirringhaus, Y. Li, Y. Wu, B. Ong, *J. Appl. Phys.* 101 (2007) 064513.
- [23] E. Chow, J. Herrmann, C.S. Barton, B. Raguse, L. Wieczorek, *Anal. Chim. Acta* 632 (2009) 135–142.
- [24] G.C. Jensen, C.E. Krause, G.A. Sotzing, J.F. Rusling, in: *PCCP* 13, 2011, pp. 4888–4894.
- [25] D.J. Lee, J.H. Oh, *Thin Solid Films* 518 (2010) 6352–6356.
- [26] K. Woo, C. Bae, Y. Jeong, D. Kim, J. Moon, *J. Mater. Chem.* 20 (2010) 3877–3882.
- [27] K. Woo, Y. Kim, B. Lee, J. Kim, J. Moon, *ACS Appl. Mater. Interfaces* 3 (2011) 2377–2382.
- [28] C.S. Choi, Y.H. Jo, M.G. Kim, H.M. Lee, *Nanotechnology* 23 (2012) 065601.
- [29] M. Grouckho, A. Kamshny, S. Magdassi, *J. Mater. Chem.* 19 (2009) 3057–3062.
- [30] K. Ankireddy, S. Vunnam, J. Kellar, W. Cross, *J. Mater. Chem. C* 1 (2013) 572–579.
- [31] Y. Tang, W. He, G. Zhou, S. Wang, X. Yang, Z. Tao, J. Zhou, *Nanotechnology* 23 (2012) 355304.
- [32] L. Polavarapu, K.K. Manga, H.D. Cao, K.P. Loh, Q.-H. Xu, *Chem. Mater.* 23 (2011) 3273–3276.
- [33] S. Jeong, H.C. Song, W.W. Lee, Y. Choi, S.S. Lee, B.-H. Ryu, *J. Phys. Chem. C* 114 (2010) 22277–22283.
- [34] B.Y. Ahn, E.B. Duoss, M.J. Motala, X. Guo, S.-I. Park, Y. Xiong, J. Yoon, R.G. Nuzzo, J.A. Rogers, J.A. Lewis, *Science* 323 (2009) 1590–1593.
- [35] K. Woo, D. Jang, Y. Kim, J. Moon, *Ceram. Int.* 39 (2013) 7015–7021.
- [36] H. Zhu, Z. Fang, C. Preston, Y. Li, L. Hu, *Energy Environ. Sci.* 7 (2014) 269–287.
- [37] M. Layani, I. Cooperstein, S. Magdassi, *J. Mater. Chem. C* 1 (2013) 3244–3249.
- [38] M. Layani, S. Magdassi, *J. Mater. Chem.* 21 (2011) 15378–15382.
- [39] R. Xu, P.D. Fleming, A. Pekarovicova, V. Bliznyuk, *J. Imaging Sci. Technol.* 49 (2005) 660–666.
- [40] Q. Huang, W. Shen, W. Song, *Appl. Surf. Sci.* 258 (2012) 7384–7388.
- [41] M. Ocwieja, Z. Adamczyk, M. Morga, A. Michna, *J. Colloid Interface Sci.* 364 (2011) 39–48.
- [42] D. Töbjörk, H. Aarnio, P. Pulkkinen, R. Bollström, A. Määttänen, P. Ihlainen, T. Mäkelä, J. Peltonen, M. Toivakka, H. Tenhu, R. Österbacka, *Thin Solid Films* 520 (2012) 2949–2955.
- [43] S.P. Chen, Z.K. Kao, J.L. Lin, Y.C. Liao, *ACS Appl. Mater. Interfaces* 4 (2012) 7064–7068.